J. Biochem. 2010;147(2):213–223 doi:10.1093/jb/mvp173

JB THE JOURNAL OF BIOCHEMISTRY

# Kinesin–Calmodulin fusion protein as a molecular shuttle

*Received September 22, 2009; accepted September 28, 2009; published online October 30, 2009*

**Hideki Shishido[1], Kiyoshi Nakazato[1], Eisaku Katayama[2], Shigeru Chaen[3] and Shinsaku Maruta[1,*]**

[1]Department of Bioinformatics, Graduate School of Engineering, Soka University, Hachioji, Tokyo 192-8577; [2]Division of Biomolecular Imaging, Institute of Medical Science, The University of Tokyo, Minato-ku, Tokyo 108-8639; and [3]Department of Integrated Sciences in Physics and Biology, College of Humanities and Sciences, Nihon University, Setagaya-ku, Tokyo 156-8550, Japan

*Shinsaku Maruta. Department of Bioinformatics, Graduate School of Engineering, Soka University, 1-236 Tangi-machi, Hachioji, Tokyo 192-8577, Japan, Tel: +81-426-91-9443, Fax: +81-426-91-9312, E-mail: maruta@soka.ac.jp

**In this study, we developed a molecular shuttle with reversible cargo-loading system by using calmodulin (CaM) and M13 peptide. We designed a kinesin (K560) chimera protein with CaM fused at the C-terminal tail region of K560 (K560–CaM). K560–CaM was expressed using an *Escherichia coli* expression system and purified. Its ATPase activity and microtubule gliding velocity were almost in a similar range as those of the wild-type kinesin. $Ca^{2+}$-dependent reversible binding of K560–CaM and M13 peptide was monitored by size-exclusion-HPLC. Rotary shadowing and electron microscopy revealed tetrameric configuration of K560–CaM in the absence of $Ca^{2+}$, while both dimeric and tetrameric configurations in the presence of $Ca^{2+}$. Further, $Ca^{2+}$-dependent change in the configuration of K560–CaM was monitored by size-exclusion-HPLC and analytical ultracentrifugation. Finally, by total internal reflection fluorescence microscopy, we successfully observed that K560–CaM transported quantum dot-conjugated M13 peptide along the microtubule in the presence of $Ca^{2+}$.**

*Keywords*: calmodulin/fusion protein/kinesin/molecular shuttle/motor protein.

*Abbreviations*: CaM, calmodulin; $Ca^{2+}$/CaM, CaM in a $Ca^{2+}$-dependent manner; EB, electron bombardment; ID, internal diameter; K560, 1–560 amino acid-residue kinesin; K560–CaM, K560 with CaM fused at the C-terminal tail region; MAP, microtubule-associated protein; MEXT, Ministry of Education, Culture, Science and Technology; MT, microtubule; NA, numerical aperture; NEMS, nanoelectromechanical systems; NIH, National Institutes of Health; Qdot, quantum dot; SEC-HPLC, size-exclusion chromatography coupled with HPLC; skMLCK, skeletal muscle myosin light chain kinase; smMLCK, smooth muscle myosin light chain kinase; TIRF, total internal reflection fluorescence; VIS, visible; YFP, yellow fluorescent protein.

Kinesin is a motor protein that moves processively along microtubules, converting the chemical energy of ATP into mechanical energy. The conventional kinesin-1, a dimeric protein, transports intracellular vesicles along axonal microtubules; structurally, it consists of two heavy and two light chains. Each heavy chain consists of an N-terminal motor domain connected via a neck linker to an α-helical coiled-coil stalk that ends in a C-terminal tail domain formed with a light chain. The motor domain is a globular domain that contains the microtubule- and ATP-binding sites. The tail domain is also a globular domain that binds the cargo such as an intracellular vesicle. Kinesin-1 moves along a microtubule in >100 consecutive 8-nm steps before dissociating (*1*, *2*).

It has been previously demonstrated that the motor domain of kinesin is very similar to that of myosin. Further, it has been suggested that these two motor proteins share a common energy-transducing mechanism. Recent X-ray crystallographic (*3–6*) and point mutation studies of the two motor proteins (*7*, *8*) have provided important information regarding mechanical transduction, suggesting that the chemical energy of ATP is mechanically transduced to generate the physical swing of the lever arm or neck linker, similar to camshaft motion, through subdomain steric interactions. The energy-conversion efficiency of kinesin-1 is known to be extremely higher than that of real machines. Therefore, it is expected that introduction of artificial switching devices into the functional sites of motor proteins may enable their use as bionanomachines.

Recently, attention is being focused on the application of molecular shuttles based on kinesin and microtubules to bionanotechnology such as to nanoelectromechanical systems (NEMS) or lab-on-a-chip devices using microtubule gliding assay in which kinesin is coated on a glass surface and microtubule gliding over the surface is observed (*9*, *10*). Regulation of the direction of microtubule gliding is necessary for the application of the kinesin-microtubule transport system to NEMS or lab-on-a-chip devices. For this regulation, linear tracks with arrowhead patterns added along them have been used (*9*, *11*). Another essential point regarding a molecular shuttle is the cargo-loading system (*12*, *13*). This system can be visualized by total internal reflection fluorescence (TIRF) microscopy (*14*). Since the intrinsic physiological mechanism underlying the selective binding of cargo to the tail domain of kinesin has not been clarified thus far, artificial binding systems have been utilized for cargo binding. For instance, in a previous study, biotin-avidin and antigen-antibody systems were used for cargo binding (*15*). These systems are known to be highly specific with extremely strong binding property. However, they have the drawback

Downloaded from http://jb.oxfordjournals.org/ at Islamic Azad University on September 28, 2012

© The Authors 2009. Published by Oxford University Press on behalf of the Japanese Biochemical Society. All rights reserved

that the shuttle cannot release the cargoes. Therefore, it is required that a molecular shuttle should have the property of reversible binding of cargo.

In virtually every eukaryotic cell, calmodulin (CaM) plays a significant role in the signaling and regulatory events occurring in many $Ca^{2+}$-dependent processes. Many of the CaM target proteins are enzymes whose activities are stimulated by binding with CaM in a $Ca^{2+}$-dependent manner ($Ca^{2+}$/CaM) (*16*, *17*). For example, $Ca^{2+}$/CaM binds to and activates smooth muscle myosin light chain kinase (smMLCK) that plays a critical role in the regulation of smooth muscle contraction (*18*). CaM is a relatively small protein consisting of 148 amino acid residues and having two globular domains that are connected to each other by a long central helix. CaM target proteins have relatively short CaM-binding peptides termed M13 peptides, IQ motifs, *etc*. It has been shown that M13 peptide, which consists of 20 residues and is a part of skeletal muscle myosin light chain kinase (skMLCK), forms a 1 : 1 complex with $Ca^{2+}$/CaM (*19–21*). In a previous study, we successfully photocontrolled the interaction of CaM with M13 peptide by using an azobenzene derivative (*22*). This photocontrolled CaM is anticipated as a useful protein in the field of bionanotechnology.

In this study, we developed a new cargo-loading system in which the cargoes reversibly bound to the shuttle depending on $Ca^{2+}$ concentration. The molecular shuttle composed of kinesin fused with CaM and cargo conjugated with M13 peptide will be applicable to other bionanomachines.

## Materials and methods

Ligation enzymes were purchased from Toyobo Co. Ltd. (Osaka, Japan), unless stated otherwise. Oligonucleotides were obtained from Sigma Genosys (Saint Louis, MO, USA). The apparatus for TALON Superflow metal affinity chromatography was procured from Clontech (Palo Alto, CA, USA). Chemical reagents were purchased from Wako Pure Chemicals (Osaka, Japan), unless stated otherwise.

### *Expression and purification of protein*

The plasmid pET21a (Novagen, Madison, WI, USA) carried a mouse conventional kinesin construct comprising residues 1–560, a 12 amino acid-residue linker, and a mouse CaM with a C-terminal 6× His tag (Fig. 1B). This plasmid (pET21a:K560–CaM) was transformed into *Escherichia coli* BL21 (DE3) pLysE cells for expression. Expressed K560–CaM was purified to homogeneity by 1-step phenyl Sepharose CL-4B (GE Healthcare, Piscataway, NJ, USA) column chromatography, as described by Persechini *et al*. (*23*). Purity was confirmed by Coomassie staining of the gel obtained after SDS–PAGE of the purified preparation (Fig. 1C). Purified K560–CaM was dialysed against 100 mM NaCl, 30 mM Tris–HCl (pH 7.5), 0.3 mM $MgCl_2$, 0.2 mM ATP and 1 mM DTT and stored at −80°C until use. M13-yellow fluorescent protein (YFP) fusion protein was prepared as described earlier (*22*). Tubulin was purified from porcine brain, as described by Hackney (*24*).

### *ATPase Activity Assay*

Microtubule-dependent ATPase activity of K560–CaM was measured at 25°C in a reaction mixture containing 0.1 μM K560–CaM, 50 mM imidazole–HCl (pH 6.7), 10 mM NaCl, 3 mM $MgCl_2$, 1 mM EGTA, 1 mM β-mercaptoethanol, 0–16 μM microtubule and 1 mM ATP. The reaction was terminated by the released Pi, the amount of which was measured according to the method described by Youngburg and Youngburg (*25*).

### *Microtubule Gliding Assay*

Microtubule gliding assay was performed according to the method described by Hancock and Howard (*26*) by using assay buffer A [50 mM K-Ace, 2.5 mM EGTA, 4 mM $MgSO_4$, 10 mM Tris-Ace (pH 7.5), 0.5 mg/ml casein, 0.5% β-mercaptoethanol and 4 μM Taxol] for all solutions. Flow cells were constructed using microscope slides, coverslips and two-sided tape. In brief, glass surfaces of the flow cells were first coated with 0.1% nitrocellulose, after which 0.5 μM motor-containing assay buffer was flowed into the cells. The motors were allowed to adhere to the glass for 5 min. Subsequently, motility solution [rhodamine-labelled microtubules (~40 nM rhodamine-labelled tubulin dimmer), 1 mM ATP, 3 mg/ml glucose, 0.02 mg/ml catalase and 0.1 mg/ml glucose oxidase] was added into the cells. Rhodamine-labelled and unlabelled tubulin were mixed in a ratio of 1 : 5 and polymerized. Fluorescent microtubule gliding was observed under epifluorescence by using Olympus BX50 microscope equipped with the 3CCD camera JK-TU53H (Toshiba, Japan).

### *Quantum dot conjugation*

Streptavidin-coated quantum dots (Qdots) emitting light at 655 nm (Invitrogen-Molecular Probes, Eugene, OR, USA) were conjugated with biotinylated M13 peptides (synthesized by GenScript, Piscataway, NJ, USA) by incubating a 1 : 1 mixture of Qdots: M13 peptides (concentration of each, 50 nM) in a solution of 30 mM Tris–HCl (pH 7.5) and 100 mM NaCl on ice for 60 min. The Qdot–M13 peptide complexes were then bound to K560–CaM by incubating an 8 : 1 mixture of Qdot–M13 : K560–CaM (K560–CaM concentration, 5 nM) in a solution of 30 mM Tris–HCl (pH 7.5), 100 mM NaCl and 1 mM $CaCl_2$ on ice for 30 min.

### *K560–CaM–Qdot motility assay*

Glass surfaces of the flow cells were first coated with 0.1% nitrocellulose, after which 0.4 μM rhodamine-labelled microtubule-containing assay buffer B [50 mM K-Ace, 2.5 mM EGTA, 4 mM $MgSO_4$, 10 mM Tris–Ace (pH 7.5), 0.5% β-mercaptoethanol and 4 μM Taxol] was flowed into the cells. The microtubules were allowed to adhere to the glass for 5 min. Subsequently, the glass surfaces and microtubules were blocked with assay buffer C (assay buffer B with 0.05 mg/ml casein, 1 mM ATP, 1 mM $CaCl_2$, 3 mg/ml glucose, 0.02 mg/ml catalase and 0.1 mg/ml glucose oxidase) and visualized. Finally, a solution of K560–CaM–Qdot complexes (K560–CaM concentration, 0.5 nM) in assay buffer C was added into the flow cells. Single molecule of Qdot was observed with an inverted microscope (Olympus IX71) equipped with TIRF optics (Olympus IX71-ARCEVA), 60× objective [numerical aperture (NA), 1.45] and an electron bombardment (EB)-CCD camera (C7190; Hamamatsu Photonics) and recorded on a hard-disk video recorder (DMR-EH55; Panasonic). Selected video frames were digitized using a frame grabber (LG3; Scion) and National Institutes of Health (NIH) Image software on a personal computer (Power Mac G4; Apple Computer, Japan). For the observation of multiple Qdot molecules, fluorescence microscope (Olympus BX50), 100× objective and 3-CCD camera (Toshiba IK-TU51CU) were used.

### *Size-exclusion chromatography coupled with HPLC*

Size-exclusion chromatography coupled with HPLC (SEC-HPLC) was performed using a TSK-GEL G3000SW column [Tosoh, Tokyo, Japan; particle size, 10 mm; internal diameter (ID), 7.5 mm; length, 30 cm; injection volume, 20 μl] with a 10–500 kDa fraction range. The samples were eluted with buffers containing 100 mM NaCl, 30 mM imidazole–HCl (pH 7.0), and 0.1 mM $CaCl_2$ or 0.1 mM EGTA at a flow rate of 1 ml/min, with absorbance monitored at 230 nm and fluorescence monitored at 527 nm (excitation wavelength, 475 nm).

### *Electron microscopy*

The specimens for electron microscopy were prepared by rotary shadowing as described earlier (*27*). In brief, K560–CaM was diluted by 12.5 μg/ml with a solution containing 0.3 M ammonium acetate, 40% glycerol and 0.1 mM $CaCl_2$ or 0.1 mM EGTA. The diluted samples of K560–CaM were immediately sprayed onto the surface of freshly cleaved mica. After rotary shadowing with platinum at an angle of 10° and coating with pure carbon, replicas were picked up onto copper grids and photographed.



Downloaded from http://jb.oxfordjournals.org/ at Islamic Azad University on September 28, 2012

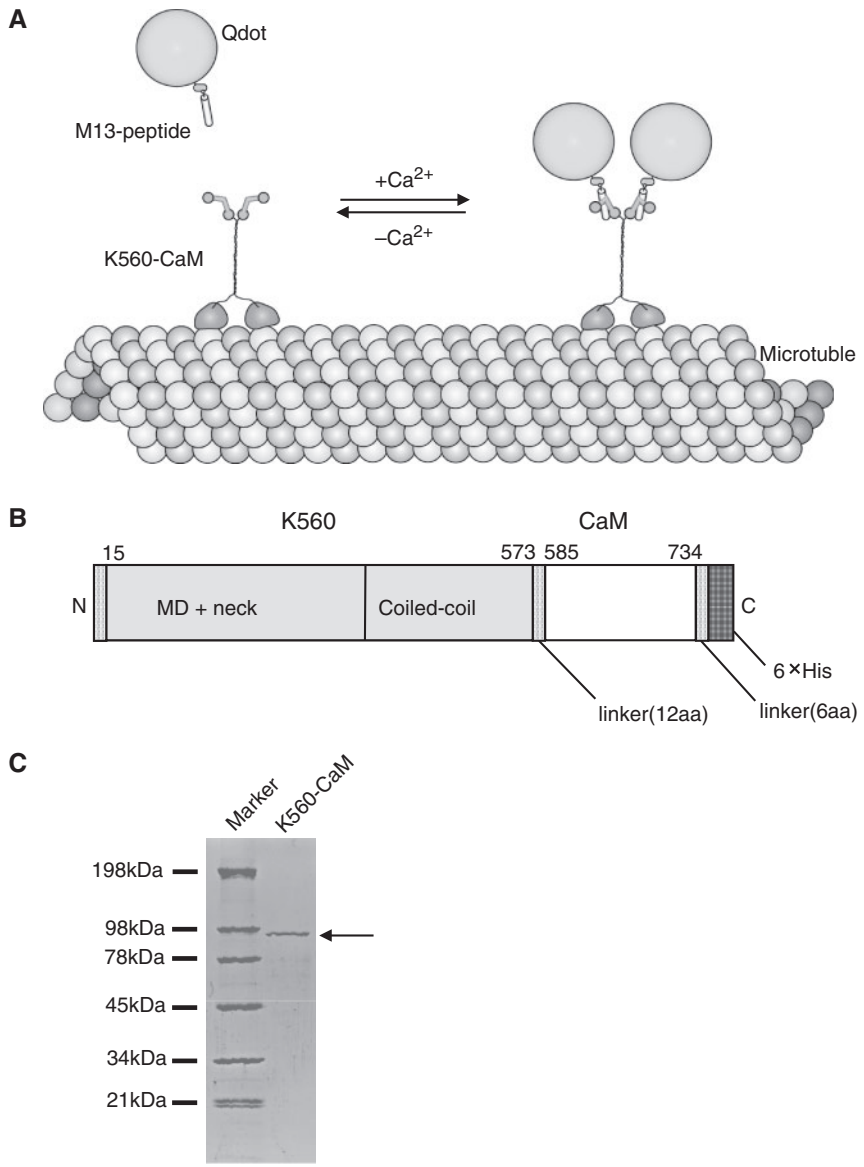


**Fig. 1 Design and preparation of K560–CaM.** (A) Schematic representation of $Ca^{2+}$-dependent reversible cargo-transport system of K560–CaM. K560–CaM fusion protein with CaM bound to the C-terminal region of 1–560 amino acid-residue kinesin (K560); Qdot, streptavidin-coated Qdot 655; M13 peptide, biotin-conjugated M13 peptide; Microtubule, fluorescent microtubule prepared from rhodamine-labelled and microtubule-associated protein (MAP)-free tubulin. CaM binds to M13 peptide in the presence of $Ca^{2+}$, and therefore, K560–CaM binds to Qdot-conjugated M13 peptide and transports Qdot along the microtubule. (B) K560–CaM composed of 746 amino acid residues that comprise 1–14 residues of peptide linker, 15–573 residues of K560, 574–584 residues of peptide linker, 585–734 residues of Ca, and 735–746 residues of peptide linker and 6× His tag. (C) Purity of K560–CaM was assessed by SDS–PAGE. First lane, molecular weight marker; second lane, purified K560–CaM. The arrow indicates K560–CaM (84.3 kDa).

#### *Analytical ultracentrifugation*

Sedimentation equilibrium experiments were performed on a Beckman XL-A analytical ultracentrifuge to investigate the configuration of K560–CaM in a mixture containing 10 μM K560–CaM, 30 mM Tris–HCl (pH 7.5), 100 mM NaCl, 0.3 mM $MgCl_2$, 0.2 mM ATP and 0.1 mM $CaCl_2$ or 0.1 mM EGTA. In all the experiments, an AN-60 Ti rotor and charcoal-filled Epon centerpiece were used. Ultracentrifugation was performed at 8,000 or 12,000 rpm. The protein concentration (C) versus radius ($r$) plots were analysed according to the following theoretical equation:

$$C(r) = C(r_b) \exp\,[MH(r^2 - r_b^2)] \quad (1)$$

where $r_b$ is the radius at the bottom of the sector, and $M$ is the molecular weight. $H$ is a constant calculated by the relationship $H = \omega^2(1 - \upsilon\rho)/2RT$, where $\upsilon$ is the partial specific volume of the protein, $\rho$ is the density of solvent, $\omega$ is the angular velocity of the rotor, $R$ is the gas constant and $T$ is the absolute temperature.

## Results

### *Preparation of K560–CaM*

For the addition of a cargo-loading system to mouse conventional kinesin in order to prepare a functional molecular shuttle, we designed K560–CaM fusion protein (Fig. 1A). The shuttle K560–CaM consists of the N-terminal motor domain, neck region, an α-helical coiled-coil region and CaM at the C-terminus (Fig. 1B). It is dimerized throughout the coiled-coil region, and CaM reversibly binds to the target M13 peptide depending on $Ca^{2+}$ concentration. K560–CaM was expressed in an *E. coli* expression system and purified by phenyl Sepharose CL-4B column chromatography according to the established methods described

Downloaded from http://jb.oxfordjournals.org/ at Islamic Azad University on September 28, 2012

**Table 1. ATPase activity of K560–CaM and microtubule gliding velocity.**

| | MT-dependent ATPase activity | | MT gliding Velocity (nm/s) |
|---|---|---|---|
| | $V_{max}$ (moles of Pi/s/moles of motor domain) | $K_m$[MT] (μM) | |
| K560–CaM | 36.63 ± 1.67 | 1.02 ± 0.16 | 872 ± 3.8 ($N = 105$) |
| K560 | 27 ± 7 (ref. *28*) | 1.1 ± 0.35 (ref. *28*) | 550 ± 140 ($N = 25–50$) (ref. *29*) |

$V_{max}$ and $K_m$[MT] were estimated from the MT-dependent ATPase activity data by using the formula $V = V_{max}/(1 + K_m[MT]/[MT])$. Data of K560–CaM and K560 are presented as mean ± SE and mean ± SD, respectively. MT, microtubule.

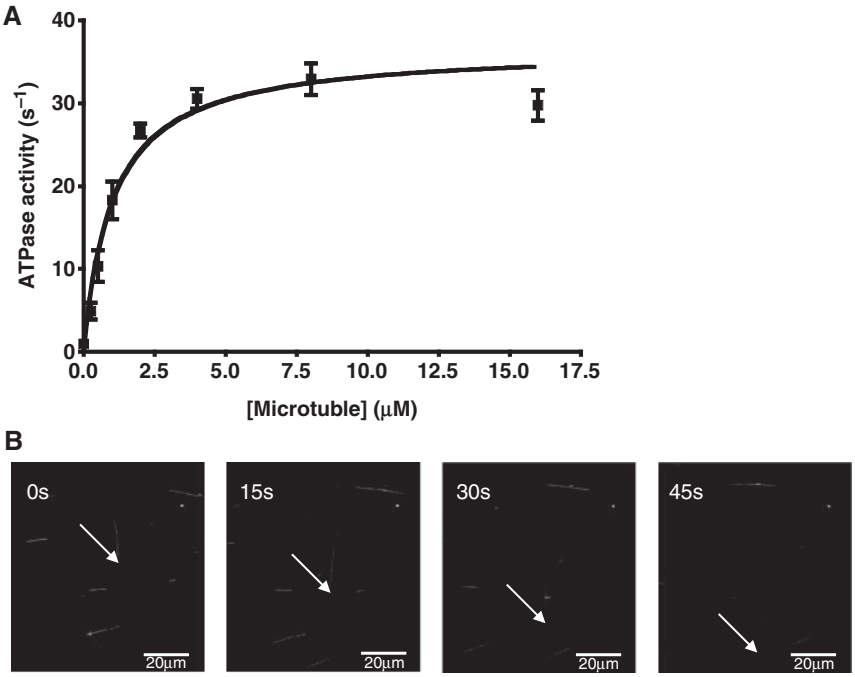


**Fig. 2 ATPase activity and microtubule gliding velocity of K560–CaM.** (A) Microtubule-dependent ATPase activity of K560–CaM was measured at 25°C in a reaction mixture containing 0.1 μM K560–CaM, 50 mM imidazole–HCl (pH 6.7), 10 mM NaCl, 3 mM $MgCl_2$, 1 mM EGTA, 1 mM β-mercaptoethanol, 0–16μM microtubule, and 1 mM ATP. (B) Fluorescence microscopy images of microtubule gliding driven by K560–CaM adsorbed on glass surface. The arrows indicate the end of the same microtubule. Scale bar, 20 μm.

in 'Materials and methods'. About 4 mg of purified K560–CaM could be obtained from 1 l of culture (Fig. 1B).

### *ATPase activity and microtubule gliding velocity of K560–CaM*

The ATPase activity of K560–CaM was measured in the presence of various concentrations of microtubules (Fig. 2A). The maximum reaction velocity ($V_{max}$), which indicates the maximum enzyme activity, was 36.63 ± 1.67 (moles of Pi/s/moles of site), and half-maximum activity was detected at the microtubule concentration ($K_m$[MT]) of 1.02 ± 0.16 μM (Table 1). These values were in a similar range as the previously reported values of the conventional kinesin ($V_{max}$, 27 ± 7 moles of Pi/s/moles of site; $K_m$[MT], 1.1 ± 0.35 μM) (*28*). Subsequently, we measured the velocity of K560–CaM-driven microtubule gliding (Fig. 2B). The fluorescent microtubules glided at a velocity of 872 ± 3.8 nm/s (Table 1). This velocity was slightly higher than that observed for the human wild-type K560 (550 ± 140 nm/s) (*29*). This result clearly demonstrated that K560–CaM maintains intrinsic motor function.

### *Interaction of K560–CaM with M13 peptide*

M13–YFP fusion protein was prepared in order to monitor the binding of K560–CaM to the target M13 peptide. We investigated the interaction between K560–CaM and M13–YFP by SEC-HPLC, monitoring the absorbance of the eluted protein (Fig. 3A and B) and the fluorescence of YFP (Fig. 3C and D). Figure 3E shows the elution times for the molecular size markers. Elution time of K560–CaM was around 5 min. The estimated molecular weight of dimeric configuration of K560–CaM from peptide sequence is 169 kDa. The sample of M13–YFP used in this study was partially degraded, which we have reported earlier (*22*). Therefore, the intact M13–YFP eluted broadly around 13–15 min. In the presence of $Ca^{2+}$, the peaks of the YFP fluorescence and K560–CaM absorbance were detected at the same time (Fig. 3A and C). On the other hand, in the absence of $Ca^{2+}$, the YFP fluorescence and K560–CaM absorbance peaks were



Downloaded from http://jb.oxfordjournals.org/ at Islamic Azad University on September 28, 2012

detected at different times (Fig. 3B and D). The peak size of M13–YFP around 13–15 min in Fig. 3C was smaller than that in Fig. 3D. These results suggested that K560–CaM binds to M13 peptide depending on $Ca^{2+}$ concentration. The peak size around 5 min in Fig. 3B was smaller than that in Fig. 3A, because M13–YFP dose not bind to K560–CaM in Fig. 3B. The elution time of the complex composed of K560–CaM and M13–YFP in the presence of $Ca^{2+}$ was 5.3 min (Fig. 3A), and elution time of K560–CaM in the absence of $Ca^{2+}$ was 5.1 min (Fig. 3B). This result suggested that estimated molecular size of K560–CaM in the absence of $Ca^{2+}$ is larger than that of complex of K560–CaM and M13–YFP in the presence of $Ca^{2+}$.

### *Configuration of K560–CaM visualized by rotary shadowing and electron microscopy*

By rotary shadowing and electron microscopy, we observed the configurations of K560–CaM in the absence and presence of $Ca^{2+}$. In the absence of $Ca^{2+}$, K560–CaM predominantly showed a tetrameric configuration, similar to a kinesin-5 family protein. A kinesin-5 family protein has one pair of motor domains located at each end of a central stalk, while wild-type K560 has an intrinsically dimeric configuration with two motor domains located at one end of a coiled-coil region (Fig. 4A). The tetrameric configuration of K560–CaM may be acquired in such a way that one pair of motor domains is located at each end of a central stalk followed by two CaMs, which are linked to the other two CaMs of K560–CaM. In the presence of $Ca^{2+}$, K560–CaM showed both dimeric and tetrameric configurations (Fig. 4B). The proportions of the dimeric and tetrameric configurations of K560–CaM in the absence or presence of $Ca^{2+}$ are summarized in Table 2. In the absence of $Ca^{2+}$, the proportions of the dimeric and tetrameric configurations of K560–CaM were 12.0% and 88.0% ($N = 160$), respectively. In the presence of $Ca^{2+}$, the proportions of the dimeric and tetrameric configurations of K560–CaM were 58.6% and 41.4% ($N = 87$), respectively. This result suggested that the equilibrium between the dimeric and tetrameric configurations of K560–CaM changes depending on $Ca^{2+}$ concentration.

### *Analysis of tetrameric and dimeric configurations of K560–CaM by SEC–HPLC*

The estimated molecular weight of tetrameric K560–CaM is two times that of dimeric K560–CaM. Therefore, the mixture of tetrameric and dimeric K560–CaM was separated by SEC–HPLC. In the absence of $Ca^{2+}$, only one peak at 5.1 min was detected (Fig. 5A), which corresponds to the tetrameric configuration of K560–CaM. This result was consistent with that obtained by rotary shadowing and electron microscopy (Fig. 4A). On the other hand, in the presence of $Ca^{2+}$, two peaks at 5.1 and 5.7 min were detected (Fig. 5B), which correspond to the tetrameric and dimeric configurations of K560–CaM, respectively. This result was also consistent with that obtained by rotary shadowing and electron microscopy (Fig. 4B). However, the peak of the mixture of K560–CaM and M13–YFP was observed as only one peak at 5.3 min in the presence of $Ca^{2+}$ (Fig. 3A). The elution time (5.3 min) in Fig. 3A was between the two elution times (5.1 and 5.7 min) in Fig. 5B. This result suggested that K560–CaM bound to M13–YFP is dimeric configuration in the presence of $Ca^{2+}$. Further, we investigated the concentration dependence of the experimentally observed proportions of the dimeric and tetrameric configurations of K560–CaM in the presence of $Ca^{2+}$ by SEC–HPLC (Fig. 5C). The proportion of tetrameric configuration of K560–CaM increased with K560–CaM concentration, reaching a maximum value of 50%.

### *Analysis of tetrameric and dimeric configurations of K560–CaM by analytical ultracentrifugation*

Analytical ultracentrifugation was also performed to investigate the configurations of K560–CaM. This technique allows the determination of radial distributions of proteins by monitoring UV absorption at 280 nm after sedimentation equilibrium. When the solution contains a single protein configuration, radial distribution is indicated by a single exponential curve (Eq. 1 in 'Materials and methods'). In the absence of $Ca^{2+}$, the radial distribution of K560–CaM was well-fitted with a single exponential curve. The apparent molecular weight of K560–CaM calculated from the data was $325 \pm 3.4$ kDa in the absence of $Ca^{2+}$, and the molecular weight of K560–CaM calculated from the amino acid composition is 84 kDa. Thus, our result strongly suggested the presence of tetrameric configuration of K560–CaM in the absence of $Ca^{2+}$. On the other hand, in the presence of $Ca^{2+}$, the radial distribution of K560–CaM was observed between individual exponential curves fitted to the molecular weights of dimeric and tetrameric K560–CaM. This result indicated that in the presence of $Ca^{2+}$, K560–CaM shows two configurations—dimeric and tetrameric configurations. The results of analytical ultracentrifugation were consistent with those of electron microscopy and SEC–HPLC (Fig. 6).

### *$Ca^{2+}$-dependent molecular shuttle*

K560–CaM is a molecular shuttle designed to load cargoes in a $Ca^{2+}$-dependent manner (Fig. 1A). Qdots were conjugated with M13 peptides by using a biotin–avidin system. Subsequently, K560–CaM was incubated with Qdot–M13 in the presence of $Ca^{2+}$ to allow binding of CaM to Qdot–M13. We observed that K560–CaM transported Qdot as cargo along a rhodamine-labelled microtubule, which adhered to the glass surface. The Qdot and rhodamine-labelled microtubule were visualized by TIRF microscopy. Since TIRF microscopy enables visualization of a specimen immediately close to the glass surface, only K560–CaM–Qdot bound to the rhodamine-labelled microtubule, and not that suspended in the flow cells, was observed. K560–CaM–Qdot moved along the rhodamine-labelled microtubule in the presence of $Ca^{2+}$ (Fig. 7A). The transport velocity and run length of K560–CaM–Qdot were $305 \pm 0.025$ nm/s (mean ± SE, $N = 48$) and $5.19 \pm 0.78$ μm (mean ± SE,

Downloaded from http://jb.oxfordjournals.org/ at Islamic Azad University on September 28, 2012

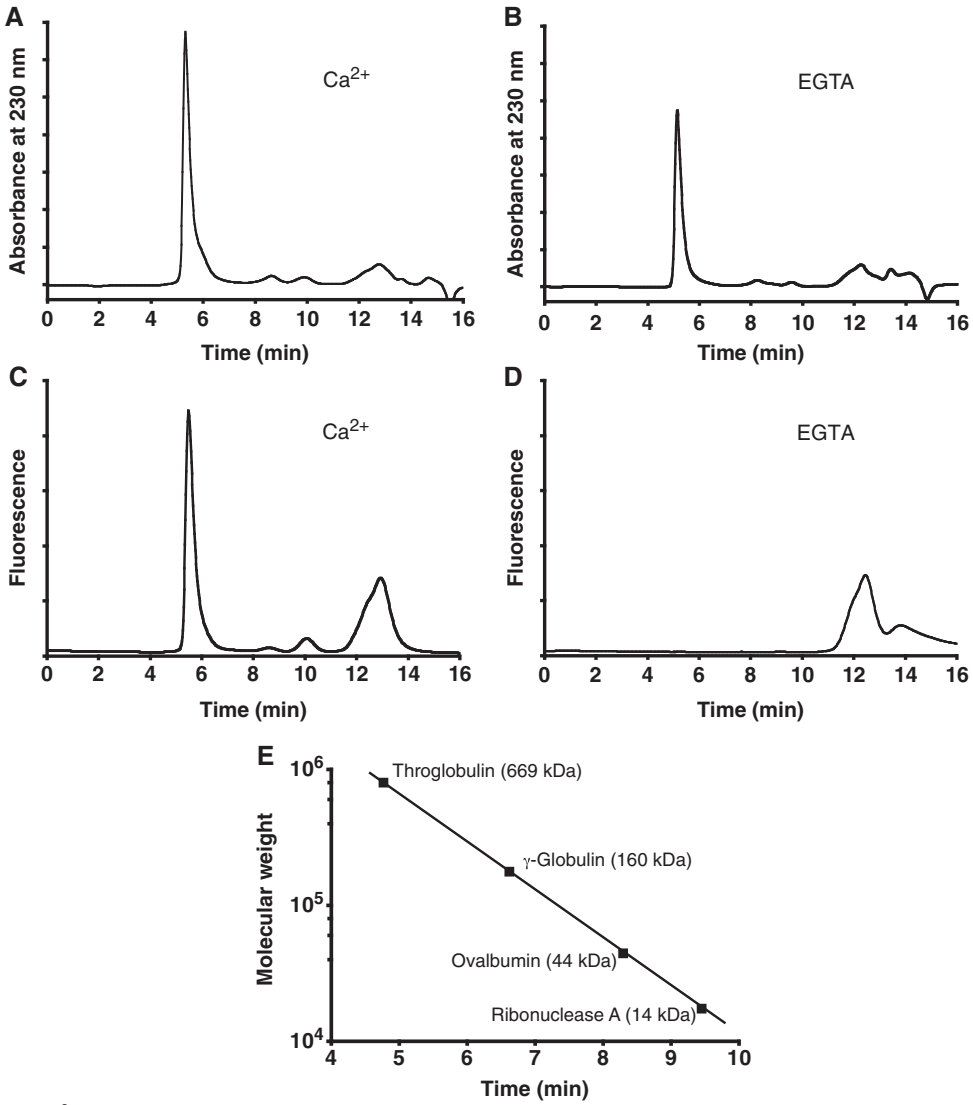


**Fig. 3 Monitoring of $Ca^{2+}$-dependent interaction of K560–CaM and M13–YFP by SEC–HPLC.** A sample of 10 μM K560–CaM and 20 μM M13–YFP in a buffer containing (A and C) 0.1 mM $CaCl_2$ or (B and D) 0.1 mM EGTA, 100 mM NaCl, 30 mM Tris–HCl (pH 7.5) was analysed by SEC–HPLC, with (A and B) absorbance monitored at 230 nm and (C and D) fluorescence monitored at 527 nm (excitation wavelength, 475 nm). (E) The elution time for the molecular size maker (Troglobulin, g-Globulin, Ovalbumin and Ribonuclease A) used SEC–HPLC.

$N = 48$), respectively (Table 3). The transport velocity of K560–CaM corresponded to that of wild-type K560, but its run length was more than that of wild-type K560 (*30*). On the other hand, in the absence of $Ca^{2+}$, K560–CaM–Qdot was not observed to move along the rhodamine-labelled microtubule (Fig. 7B). These results indicated that K560–CaM transports Qdot along a microtubule only in the presence of $Ca^{2+}$.

Reversible $Ca^{2+}$ dependent cargo-loading system was achieved by changing the $Ca^{2+}$ concentration in the flow cell as shown in Fig. 8. K560–CaM was adsorbed onto the fluorescently unlabelled microtubule adhered on the glass surface in flow cell using non-hydrolyzable ATP analogue, AMP–PNP which stabilize the microtubule binding state of kinesin (Fig. 8A). Subsequently, Qdot–M13 was added in the presence of $Ca^{2+}$ to be loaded on K560–CaM adsorbed on the microtubule. As shown in Fig. 8B, the fluorescence of Qdot–M13 loaded onto K560–CaM along a microtubule was observed after washing excess unbound Qdot–M13. When the $Ca^{2+}$ solution in the flow cell was replaced by the $Ca^{2+}$ free solution, Qdot–M13 was unloaded (Fig. 8C). Even after the several times alternate exchange of the solution in the flow cell with $Ca^{2+}$ and EGTA solutions, the K560–CaM adsorbed onto microtubule by AMP–PNP showed stable $Ca^{2+}$-dependent cargo loading (Fig. 8B–F). When excess ATP was added into the flow cell, K560–CaM–Qdot started to move along the microtubule (Fig. 8G). Interestingly, 145 s later, K560–CaM–Qdot accumulated at plus end of microtubule and showed fluorescent clumps (Fig. 8H). And the Qdot–M13 dissociated from K560–CaM in the clumps by removing $Ca^{2+}$ from the flow cell (Fig. 8I). These results clearly demonstrated that the K560–CaM as molecular shuttle is capable of $Ca^{2+}$-dependent reversible cargo loading.

Downloaded from http://jb.oxfordjournals.org/ at Islamic Azad University on September 28, 2012

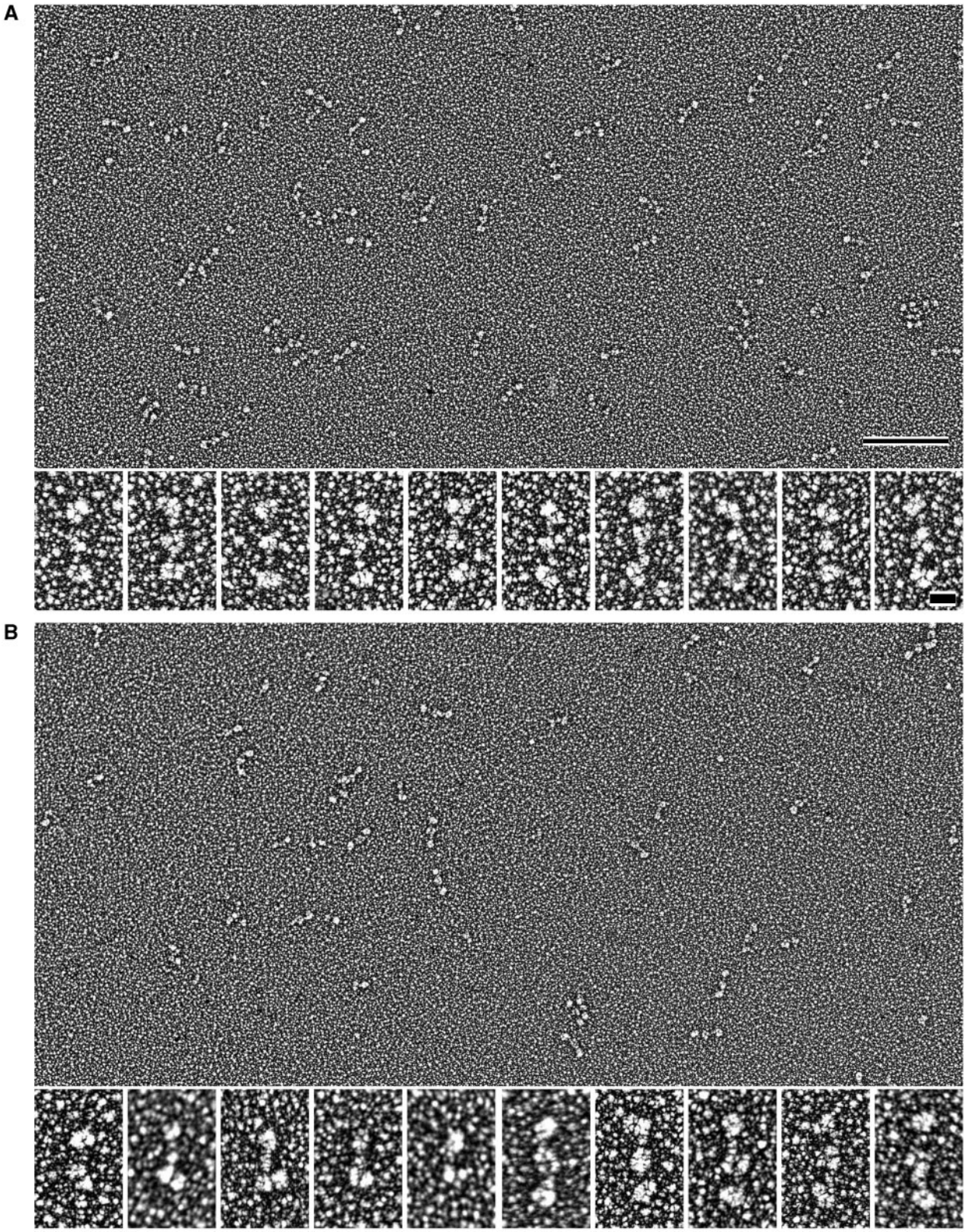


**Fig. 4 Rotary shadowing and electron microscopy of $Ca^{2+}$-dependent change in K560–CaM configuration**. (A, top) General view of K560–CaM conformers in the absence of $Ca^{2+}$. Scale bar, 200 nm. (A, bottom) Gallery of typical K560–CaM conformers in the absence of $Ca^{2+}$. Scale bar, 20 nm. In the absence of $Ca^{2+}$, K560–CaM showed a tetrameric configuration, similar to a kinesin-5 family protein. (B, top) General view of K560–CaM conformers in the presence of $Ca^{2+}$. (B, bottom) Gallery of typical K560–CaM conformers in the presence of $Ca^{2+}$. In the presence of $Ca^{2+}$, K560–CaM showed both tetrameric and dimeric configurations, similar to a kinesin-1 family protein.

Downloaded from http://jb.oxfordjournals.org/ at Islamic Azad University on September 28, 2012

**Table 2. Proportions of $Ca^{2+}$-dependent configurations of K560–CaM visualized by electron microscopy after rotary shadowing.**

| | Dimer | Tetramer |
|---|---|---|
| EGTA ($N = 160$) | 12.00% | 88.00% |
| $Ca^{2+}$ ($N = 87$) | 58.60% | 41.40% |

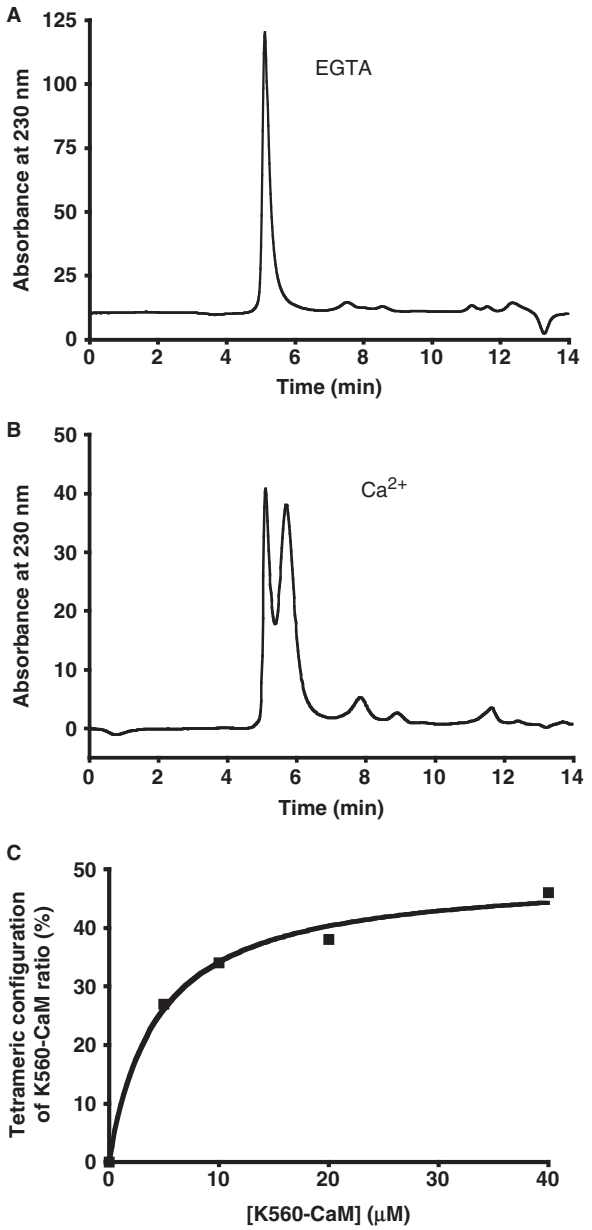


**Fig. 5 Separation of a mixture of dimeric and tetrameric K560–CaM by SEC–HPLC.** A sample of 10 μM K560–CaM in a buffer containing (A) 0.1 mM EGTA or (B) 0.1 mM $CaCl_2$, 100 mM NaCl and 30 mM Tris–HCl (pH 7.5) was analysed by SEC–HPLC, with absorbance monitored at 230 nm. (C) Concentration dependence of the experimentally observed proportions of the dimeric and tetrameric configurations of K560–CaM in the presence of $Ca^{2+}$ was determined by SEC–HPLC.

## Discussion

In this study, we developed a reversible cargo-loading system for the K560–CaM molecular shuttle, employing $Ca^{2+}$-dependent CaM–M13 peptide binding. In a previous study, biotin–avidin and antigen–antibody systems were employed for cargo loading (*15*). Although the systems are highly specific with strong binding property, they have the drawback of binding cargoes irreversibly. It is very important for a molecular shuttle that it transports cargoes continuously and releases the loaded cargoes at the destination. Therefore, development of a molecular shuttle that can bind to and release cargos reversibly by exogenous stimuli is desired.

CaM is well-known as a $Ca^{2+}$-binding protein and is one of the key regulatory proteins of cell signal transduction pathways. The activities of numerous enzymes involved in cell function are regulated by CaM, and the regulatory mechanism has been elucidated at the molecular level. $Ca^{2+}$/CaM binds to the well-conserved binding region M13 in CaM-dependent enzymes, resulting in the stimulation of the enzyme activities. The binding is highly reversible depending on the $Ca^{2+}$ concentration. Moreover, CaM and its target M13 peptide are structurally very stable and can be readily fused with a motor protein by a molecular biological technique. Therefore, $Ca^{2+}$-dependent CaM–M13 interaction is a suitable cargo-loading mechanism for a molecular shuttle as a device of NEMS or lab-on-a-chip.

In fact, as shown in Fig. 7A, Qdot–M13 was loaded as a cargo on K560–CaM and transported along microtubules in the presence of $Ca^{2+}$. On the other hand, in the absence of $Ca^{2+}$, the cargo was not loaded on K560–CaM (Fig. 7B). For actual application as a molecular shuttle, K560–CaM should bind the target cargo in the presence of $Ca^{2+}$, transport it along a microtubule, and then release the transported cargo at the destination by removal of $Ca^{2+}$. For the binding and release of the target cargo, $Ca^{2+}$ may be added and removed by using a $Ca^{2+}$ gradient solvent in flow channel or a caged $Ca^{2+}$ chelator and caged $Ca^{2+}$. In this study, $Ca^{2+}$-dependent reversible cargo loading system using K560–CaM and Qdot–M13 was actually achieved by alternate exchange of the solution in the flow cell with $Ca^{2+}$ and EGTA solutions (Fig. 8). Another possible approach may be the use of photocontrolled CaM. We have previously demonstrated that the functions of CaM mutants with photochromic compounds incorporated in their functional region were reversibly controlled by UV–visible (VIS) light irradiation (*22*). Therefore, it is expected that interaction of K560-photochromic CaM with the target peptide can be photocontrolled by UV–VIS light irradiation.

In previously reported molecular shuttle systems utilizing kinesin and microtubules, the microtubule functions as a shuttle and transports cargoes on a kinesin-adsorbed glass surface (*9*, *10*). It is known that the microtubules glide in random directions on the kinesin-adsorbed glass surface. Therefore, a circuit of spiral or arrowhead pattern was added in this system to facilitate unidirectional movement of microtubules (*11*). Special equipment and room are required to prepare such a circuit, which is inconvenient; moreover, the unidirectionality of movement is not 100%. On the other hand, our system uses cargo-loading



Downloaded from http://jb.oxfordjournals.org/ at Islamic Azad University on September 28, 2012

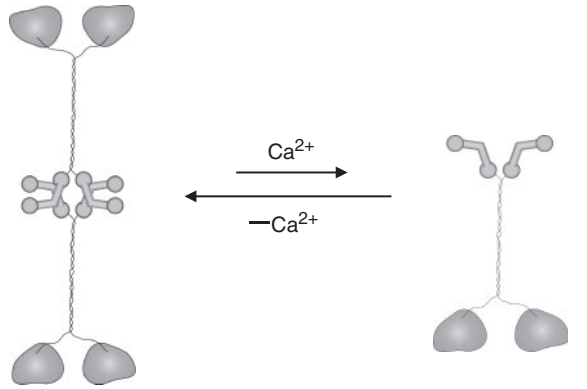


**Fig. 6 Proposed model of $Ca^{2+}$-induced change in K560–CaM configuration.** In the absence of $Ca^{2+}$, K560–CaM shows tetrameric configuration, while in the presence of $Ca^{2+}$, it shows both dimeric and tetrameric configurations. This configuration change of K560–CaM-dependent on $Ca^{2+}$ is equilibrium relation.

kinesin as a shuttle, which moves on microtubules adsorbed on a glass surface. Therefore, 100% unidirectionality of movement towards the plus end of the microtubules has been achieved. Moreover, since a single-kinesin molecule shuttle is smaller than a microtubule shuttle, it is possible to transport cargoes precisely on a submicroscopic tip.

K560–CaM showed similar or slightly stronger ATPase activity and microtubule gliding, compared

**Table 3. Single-molecule transport velocity and run length of K560–CaM.**

| | Transport velocity (nm/s) | Run length (μm) |
|---|---|---|
| K560–CaM[a] | 305 ± 25 ($N = 48$) | 5.19 ± 0.78 ($N = 48$) |
| K560 (ref. *30*) | 310 ± 70 ($N > 70$) | 0.93 ± 0.07 ($N > 70$) |

[a]Data of K560–CaM and K560 are presented as mean ± SE and mean ± SD, respectively.

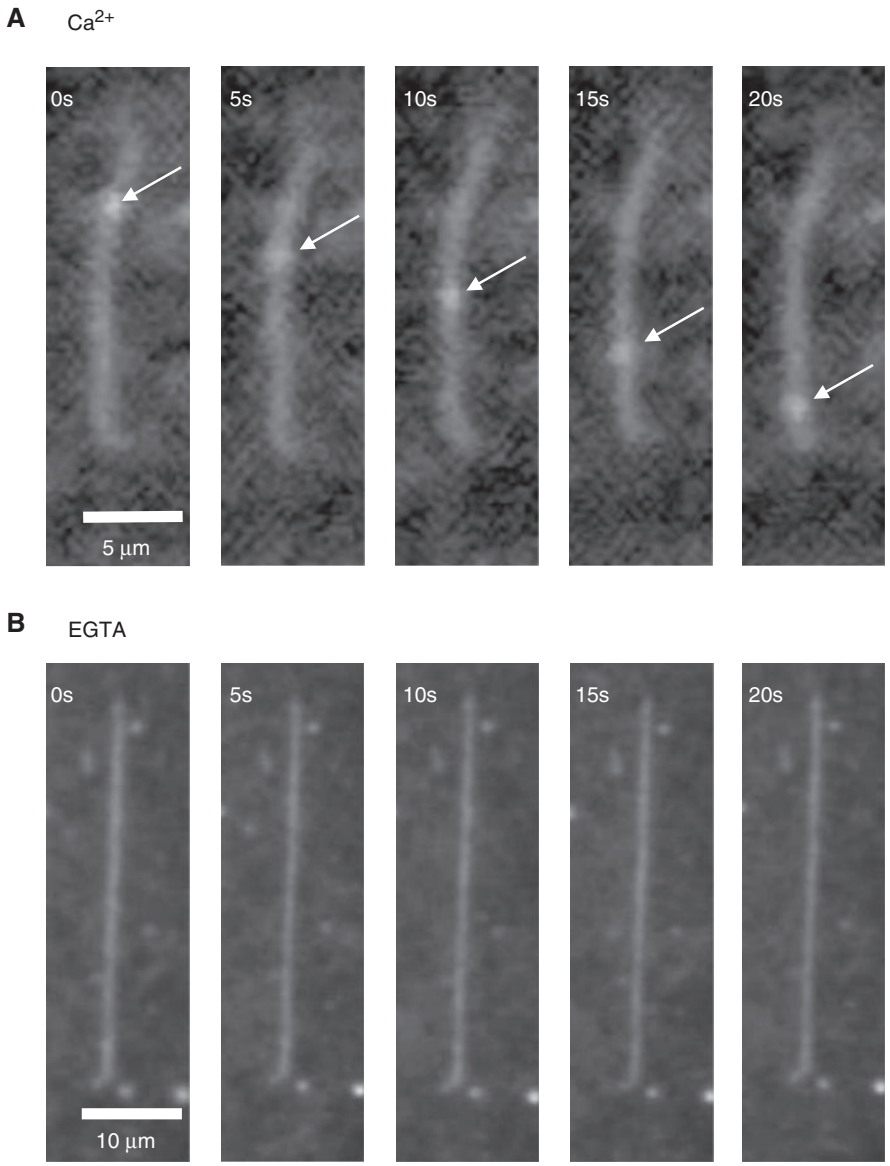


**Fig. 7 Qdot transportation by K560–CaM along a microtubule in the presence of $Ca^{2+}$.** TIRF microscopy of Qdot 655-conjugated K560–CaM (indicated by arrow) showed movement along the rhodamine-labelled microtubule. Concentrations: K560–CaM, 0.5 nM; Qdot 655, 4 nM; biotinylated M13 peptide, 4 nM; MgATP, 4 mM; (A) $CaCl_2$, 1 mM; (B) EGTA, 1 mM. Images in a single frame at different time points are shown. Scale bar: (A) 5 μm and (B) 10 μm.

Downloaded from http://jb.oxfordjournals.org/ at Islamic Azad University on September 28, 2012

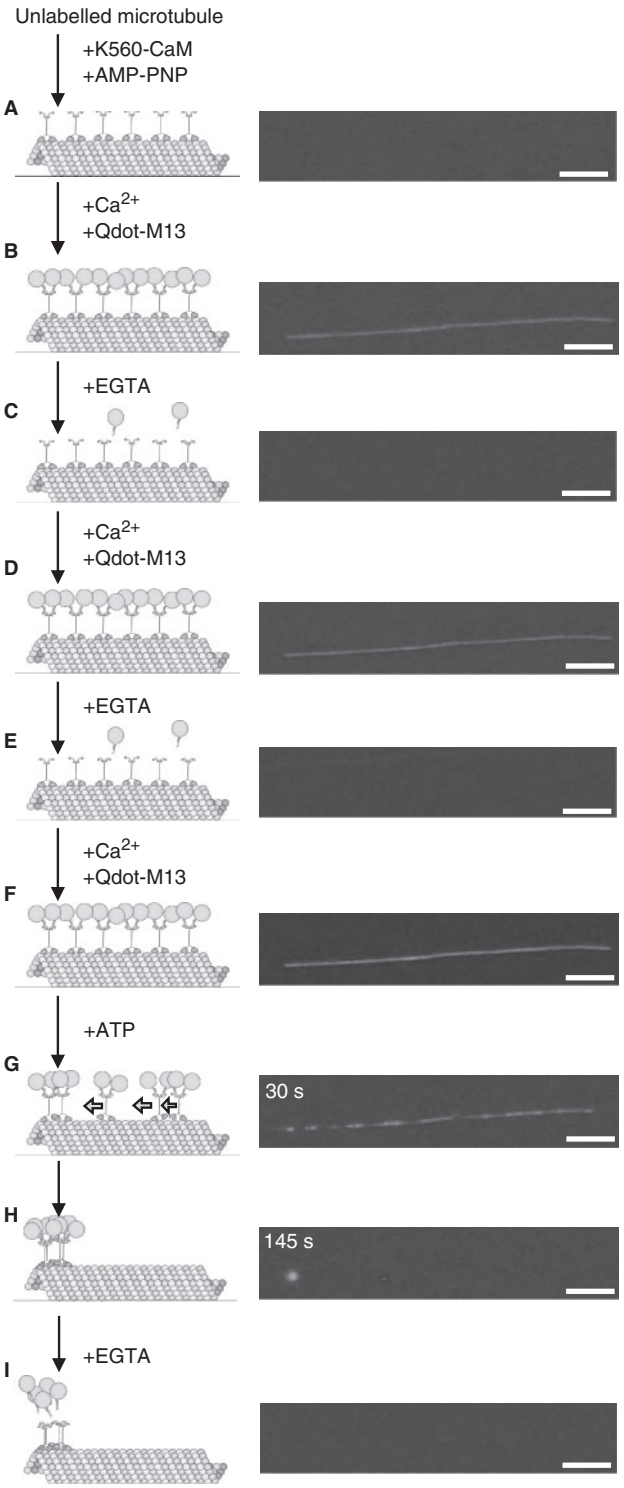


**Fig. 8 $Ca^{2+}$ dependent reversible cargo loading of K560–CaM.** (Light) Schematic illustration and (Right panel) fluorescence microscopy images of Qdot-conjugated K560–CaM on the microtubule in flow cells in the presence or absence of $Ca^{2+}$. (A) 350 nM K560–CaM was adsorbed onto the fluorescently unlabelled microtubule in the presence of 5 mM AMP–PNP; (B) 20 nM Qdot 655-biotinylated M13 peptide was added to be loaded on the K560–CaM in the presence of 10 μM $CaCl_2$ and 5 mM AMP-PNP; (C) the solution in the flow cell was replaced by the solution containing 1 mM EGTA and 5 mM AMP-PNP to unload the Qdot.; (D) same procedure to B; (E) same procedure to C; (F) same procedure to B; (G) after washing excess unbound Qdot, 5 mM ATP was added in the presence of 10 μM $CaCl_2$. (Right panel of G and H) Images in a single frame at different time points 30 and 145 s after adding ATP; (I) the solution in the flow cell was replaced by the solution containing 1 mM EGTA. Scale bar: 10 μm.

with the wild-type K560 (Table 1). This suggests that the CaM moiety fused to the C-terminal of K560 does not affect the intrinsic motor activity of K560. However, interestingly, K560–CaM showed a change in the higher-order structure depending on $Ca^{2+}$ concentration. Rotary shadowing and electron microscopy clearly demonstrated that K560–CaM predominantly showed tetrameric configuration in the absence of $Ca^{2+}$ (Fig. 4A). On the other hand, in the presence of $Ca^{2+}$, the proportion of the tetrameric configuration was significantly decreased (Fig. 4B). It is known that monomeric and dimeric configurations of CaM exist in equilibrium (*31*); hence, formation of the tetrameric configuration of K560–CaM seems to be due to the interaction of the CaM moieties of two K560–CaM dimers. In fact, the concentration-dependent proportions of the tetrameric and dimeric configurations of K560–CaM (Fig. 5C) are similar to those of the dimeric and monomeric configurations of CaM, respectively (*31*). From the results of analytical ultracentrifugation, it was confirmed that $Ca^{2+}$-dependent configurational change of K560–CaM is in the equilibrium relation between tetramer to dimer (Fig. 6). It is known that wild-type kinesin-5 shows a physiologically useful tetrameric bipolar configuration (*32*). The bipolar configuration of kinesin-5 contributes to the bipolar organization of mitotic spindles by crosslinking and sliding of overlapping interpolar microtubules (*32*, *33*). We examined whether K560–CaM induces microtubule bundling as perfectly as kinesin-5. As expected, K560–CaM induced bundling of microtubules (data not shown). Artificial $Ca^{2+}$-dependent formation of tetrameric configuration of motor proteins using CaM may contribute to the field of bionanotechnology as a device.

In conclusion, we prepared K560–CaM fused protein as a molecular shuttle with a $Ca^{2+}$-dependent reversible cargo-loading system. It is anticipated that allocation of new functions to K560–CaM would make it a more functional molecular shuttle.

**Funding**

This work was supported by the Grant-in-Aid for Scientific Research in Innovative Area from the Ministry of Education, Culture, Science and Technology (MEXT); and the Nihon University Individual Research Grant for 2008 to S.C.

**Conflict of interest**

None declared.

## References

1. Howard, J., Hudspeth, A.J., and Vale, R.D. (1989) Movement of microtubules by single kinesin molecules. *Nature* **342**, 154–158
2. Block, S.M., Goldstein, L.S., and Schnapp, B.J. (1990) Bead movement by single kinesin molecules studied with optical tweezers. *Nature* **348**, 348–352
3. Kull, F.J., Sablin, E.P., Lau, R., Fletterick, R.J., and Vale, R.D. (1996) Crystal structure of the kinesin motor domain reveals a structural similarity to myosin. *Nature* **380**, 550–555
4. Rayment, I., Rypniewski, W.R., Schmidt-Base, K., Smith, R., Tomchick, D.R., Benning, M.M., Winkelmann, D.A., Wesenberg, G., and Holden, H.M.



Downloaded from http://jb.oxfordjournals.org/ at Islamic Azad University on September 28, 2012

(1993) Three-dimensional structure of myosin subfragment-1: a molecular motor. *Science* **261**, 50–58
5. Fischer, A.J., Smith, C.A., Thoden, J.B., Smith, R., Sutoh, K., Holden, H.M., and Rayment, I. (1995) X-ray structures of the myosin motor domain of *Dictyostelium discoideum* complexed with $MgADPBeF_x$ and $MgADPAlF_4^-$. *Biochemistry* **34**, 8960–8972
6. Dominguez, R., Freyzon, Y., Trybus, K.M., and Cohen, C. (1998) Crystal structure of a vertebrate smooth muscle myosin motor domain and its complex with the essential light chain: Visualization of the pre-power stroke state. *Cell* **94**, 559–571
7. Klumpp, L.M., Brendza, K.M., Gatial, J.E., Hoenger, A., Saxton, W.M., and Gilbert, S.P. (2004) Microtubule-kinesin interface mutants reveal a site critical for communication. *Biochemistry* **43**, 2792–2803
8. Yun, M., Zhang, X., Park, C.G., and Endow, S.A. (2001) A structural pathway for activation of the kinesin motor ATPase. *EMBO J.* **20**, 2611–2618
9. Hess, H. and Vogel, V. (2001) Molecular shuttles based on motor proteins: active transport in synthetic environments. *J. Biotechnol.* **82**, 67–85
10. Hess, H., Bachand, G.D., and Vogel, V. (2004) Powering nanodevices with biomolecular motors. *Chemistry* **10**, 2110–2116
11. Hiratsuka, Y., Tada, T., Oiwa, K., Kanayama, T., and Uyeda, T.Q. (2001) Controlling the direction of kinesin-driven microtubule movements along microlithographic tracks. *Biophys. J.* **81**, 1555–1561
12. Jia, L., Moorjani, S.G., Jackson, T.N., and Hancock, W.O. (2004) Microscale transport and sorting by kinesin molecular motors. *Biomed. Microdevices* **6**, 67–74
13. Muthukrishnan, G., Hutchins, B.M., Williams, M.E., and Hancock, W.O. (2006) Transport of semiconductor nanocrystals by kinesin molecular motors. *Small* **2**, 626–630
14. Pierce, D.W. and Vale, R.D. (1998) Assaying processive movement of kinesin by fluorescence microscopy. *Methods Enzymol.* **298**, 154–171
15. Ramachandran, S., Ernst, K.H., Bachand, G.D., Vogel, V., and Hess, H. (2006) Selective loading of kinesin-powered molecular shuttles with protein cargo and its application to biosensing. *Small* **2**, 330–334
16. Chin, D. and Means, A.R. (2000) Calmodulin: a prototypical calcium sensor. *Trends Cell Biol.* **10**, 322–328
17. Persechini, A. and Stemmer, P.M. (2002) Calmodulin is a limiting factor in the cell. *Trends Cardiovasc. Med.* **12**, 32–37
18. Kamm, K.E. and Stull, J.T. (2001) Dedicated myosin light chain kinases with diverse cellular functions. *J. Biol. Chem.* **276**, 4527–4530
19. Blumenthal, D.K., Takio, K., Edelman, A.M., Charbonneau, H., Titani, K., Walsh, K.A., and Krebs, E.G. (1985) Identification of the calmodulin-binding domain of skeletal muscle myosin light chain kinase. *Proc. Natl Acad. Sci. USA* **82**, 3187–3191
20. Meador, W.E., Means, A.R., and Quiocho, F.A. (1992) Target enzyme recognition by calmodulin: 2.4 A structure of a calmodulin-peptide complex. *Science* **257**, 1251–1255
21. Meador, W.E., Means, A.R., and Quiocho, F.A. (1993) Modulation of calmodulin plasticity in molecular recognition on the basis of x-ray structures. *Science* **262**, 1718–1721
22. Shishido, H., Yamada, M.D., Kondo, K., and Maruta, S. (2009) Photocontrol of calmodulin interaction with target peptides using azobenzene derivative. *J. Biochem.* **146**, 581–590
23. Persechini, A., Blumenthal, D.K., Jarrett, H.W., Klee, C.B., Hardy, D.O., and Kretsinger, R.H. (1989) The effects of deletions in the central helix of calmodulin on enzyme activation and peptide binding. *J. Biol. Chem.* **264**, 8052–8058
24. Hackney, D.D. (1988) Kinesin ATPase: rate-limiting ADP release. *Proc. Natl Acad. Sci. USA* **85**, 6314–6318
25. Youngburg, G.E and Youngburg, M.V. (1930) A system of blood phosphorus analysis. *J. Lab. Clin. Med.* **16**, 158–166
26. Hancock, W.O. and Howard, J. (1998) Processivity of the motor protein kinesin requires two heads. *J. Cell Biol.* **140**, 1395–1405
27. Katayama, E. and Ikebe, M. (1995) Mode of caldesmon binding to smooth muscle thin filament: possible projection of the amino-terminal of caldesmon from native thin filament. *Biophys. J.* **68**, 2419–2428
28. Woehlke, G., Ruby, A.K., Hart, C.L., Ly, B., Hom-Booher, N., and Vale, R.D. (1997) Microtubule interaction site of the kinesin motor. *Cell* **90**, 207–216
29. Case, R.B., Pierce, D.W., Hom-Booher, N., Hart, C.L., and Vale, R.D. (1997) The directional preference of kinesin motors is specified by an element outside of the motor catalytic domain. *Cell* **90**, 959–966
30. Romberg, L., Pierce, D.W., and Vale, R.D. (1998) Role of the kinesin neck region in processive microtubule-based motility. *J. Cell Biol.* **140**, 1407–1416
31. Lafitte, D., Heck, A.J., Hill, T.J., Jumel, K., Heading, S.E., and Derrick, P.J. (1999) Evidence of noncovalent dimerization of calmodulin. *Eur. J. Biochem.* **261**, 337–344
32. Kashina, A.S., Baskin, R.J., Cole, D.G., Wedaman, K.P., Saxton, W.M., and Scholey, J.M. (1996) A bipolar kinesin. *Nature* **379**, 270–272
33. Sharp, D.J., McDonald, K.L., Brown, H.M., Matthies, H.J., Walczak, C., Vale, R.D., Mitchison, T.J., and Scholey, J.M. (1999) The bipolar kinesin, KLP61F, cross-links microtubules within interpolar microtubule bundles of *Drosophila* embryonic mitotic spindles. *J. Cell Biol.* **144**, 125–138

Downloaded from http://jb.oxfordjournals.org/ at Islamic Azad University on September 28, 2012